

Technical Report

Enhanced dark field microscopy for rapid artifact-free detection of nanoparticle binding to *Candida albicans* cells and hyphae

Heidi Weinkauff and Byron F. Brehm-Stecher

Rapid Microbial Detection and Control Laboratory, Department of Food Science and Human Nutrition, Iowa State University, Ames, IA, USA

We surveyed a panel of 13 metal nanoparticle (NP) catalysts for their antifungal activities against *Candida albicans* ATCC 90028. Initial characterization using scanning electron microscopy (SEM) suggested that our ability to detect NP binding to *Candida* surfaces with this method was impeded by preparation artifacts. As an alternative method for visualizing NP binding, we used an enhanced dark field illumination system (CytoViva®) attached to a standard light microscope. When viewed using this system, all NP produced intense optical signals due to resonant light scattering. To assay binding, NP were allowed to interact with *C. albicans* hyphae and cells in spent RPMI broth for 15 min with gentle inversion, followed by viewing with the CytoViva® system. The antifungal efficacy of NP preparations was determined separately using a 24-h broth microdilution test. For single-metal NP, observations of binding at 15 min made *via* CytoViva® corresponded to antifungal efficacy at 24 h, with the most antifungal NP yielding complete coverage of hyphal surfaces. Our work suggests the utility of visual screening using the CytoViva® system for rapid, simple and artifact-free viewing of NP-cell interactions in support of antimicrobial screening efforts. This approach provides a quick and accessible alternative to SEM for imaging of NP-cell interactions.

Received 21 December 2008

Revised 3 April 2009

Accepted 18 April 2009

Keywords: Antifungal · *Candida albicans* · Dark field microscopy · Metal nanoparticles · Resonant light scattering

1 Introduction

Certain metals, including copper and silver, have long been known to possess broad-spectrum antimicrobial activities in ionic or macrometallic forms [1–3]. Recent work has also focused on the antimicrobial efficacy of these metals in nanoparticulate form [4]. Due to the rapid growth of the nanotech sector in the past few years, there is now

a ready commercial supply of “off-the-shelf” nanomaterials produced or marketed for use in fields as diverse as consumer electronics, alternative energy production, optics and national defense [5]. We undertook this study to examine the potential of some commercially available metal nanoparticle (NP) catalysts as novel antifungal agents, using *Candida albicans* as a model organism. We theorized that if new types of antifungally effective NP could be identified, and if potential issues of undesirable migration or toxic off-target effects could be minimized, these NP might have valuable applications as components of antifungal materials or surfaces, or in therapeutic applications, either alone or in synergistic combination with additional agents. The greatest focus of published work on NP as antimicrobials has been on metals such as silver, gold and copper. However, NP catalysts comprised of other metals are commercially available, including some that have not yet been examined in detail for

Correspondence: Dr. Byron F. Brehm-Stecher, 2312 Food Sciences Building, Iowa State University, Ames, IA 50011, USA
E-mail: byron@iastate.edu
Fax: +1-515-294-8181

Abbreviations: EDFM, enhanced dark field microscopy; MIC, minimum inhibitory concentration; NP, nanoparticle(s); ppm, parts per million; SEM, scanning electron microscopy; SPIM, single-(selective-) plane imaging microscopy

their antimicrobial effects. Apart from single-metal NP, these include novel metal alloys.

Silver NP have been shown to exert biological effects on *Escherichia coli* that are similar to those of ionic silver, but that occur at much lower (nanomolar vs. micromolar) concentrations [6]. These effects include collapse of membrane potential and depletion of adenosine triphosphate (ATP) [6]. For *Candida albicans*, treatment with silver NP leads to perturbation of normal membrane function and cell-cycle arrest [7]. Potential mechanisms underlying these antimicrobial effects could include direct complexation of NP with and inactivation of critical cell components such as the enzymes forming the respiratory chain or other key macromolecules (DNA, other proteins, etc.) [6]. Indirect “proximity” effects are also possible. Examples include catalytic activities such as generation of reactive oxygen species [4], localized release of toxic metal ions, or disruption of the electron transport chain through binding of these dense sources of free electrons at or near the membrane. Regardless of the mechanism, direct physical contact of silver or other metal NP with cell surfaces is expected to be important in mediating their antimicrobial activities. Methods for direct observation of NP interactions with microbial surfaces could help establish such binding-activity linkages. This report summarizes our investigation of the antifungal effects of these 13 metal NP catalysts, our initial attempts at detecting and characterizing NP binding *via* scanning electron microscopy (SEM) and our subsequent exploration of enhanced dark field microscopy for detecting NP-fungal interactions as a potential alternative means for rapid estimation of NP antifungal efficacy.

2 Materials and methods

2.1 Nanoparticles

Seven single-metal NP (cobalt, copper, silver, nickel, manganese, palladium, iron) and six alloy NP (cobalt/nickel/manganese, cobalt/iron, copper/indium, copper/silver, manganese/iron, nickel/iron) were examined. For alloy NP, individual metals were present in ratios of 1:1 (bimetallic alloys) or 1:1:1 (trimetallic alloy). These NP, sold commercially as catalysts for alternative energy applications, were produced by vapor condensation in an inert gas atmosphere. NP were received as uniform black powders from QuantumSphere (Santa Ana, CA). Stock suspensions (5% w/v) of all NP were made in dimethylformamide (DMF), which was de-

termined through initial investigation to facilitate their even suspension in aqueous media.

2.2 Fungal culture

Candida albicans ATCC 90028 was grown overnight at 35°C in RPMI 1640 broth (Sigma-Aldrich, St. Louis, MO) according to CLSI guidelines (M27-A).

2.3 Determination of minimum inhibitory concentration

The minimum inhibitory concentration (MIC) was determined against *C. albicans* for each type of metal NP using a broth microdilution assay. These tests were performed using a Bioscreen C Microbiological Reader (Growth Curves, Piscataway, NJ) according to the method of Lambert *et al.* [8]. Briefly, serial half-fold dilutions of NP in DMF were made horizontally across microtiter plates into RPMI-1640, yielding NP concentrations ranging from 2000 to 7.81 µg/mL (or parts per million, ppm). For the most active NP, additional dilutions were included as needed. DMF-only treatments were also included to control for possible antifungal effects of this solvent. *C. albicans* cultures were added at a final inoculum of 10⁵ colony forming units (CFU)/well and plates were incubated in the Bioscreen at 35°C for 24 h, with shaking for 60 s prior to each reading in order to resuspend settled particles. The instrument measured the optical density (600 nm) of all wells, at 15-min intervals. For each type of NP, MIC was defined as the lowest concentration of NP that completely inhibited growth (OD increase ≤0.05) after 24 h [9].

2.4 Nanoparticle binding conditions

Overnight cultures of *C. albicans* (a mixture of hyphae and yeast cells) were suspended in fresh RPMI broth to yield a final concentration of 10⁷ CFU/mL. NP were added to these suspensions at a single concentration of 250 ppm and cell-NP mixtures were incubated for 15 min with gentle inversion on a Sarmix GM1 rotating mixer (Sarstedt, Newton, NC). Large particle aggregates, if present, were allowed to settle out for 5 min and hyphae or cells remaining in the supernatant were examined *via* SEM or dark field microscopy as described below.

2.5 Scanning electron microscopy

For SEM, cell-NP mixtures were made as described above and then fixed for 15 min at 25°C with the addition of EM-grade glutaraldehyde (2.5% final con-

centration, Sigma-Aldrich), followed by resuspension in phosphate buffered saline (PBS). Samples were shipped in PBS to the University of Iowa's Central Microscopy Research Facility (Iowa City, IA) for additional preparation prior to SEM. Briefly, a drop of the fixed sample was applied to a poly-L-lysine-treated silicon chip, allowed to adhere for 5 min, and then fixed further in 1% osmium tetroxide, followed by dehydration in an ethanol series, sputter coating and viewing *via* SEM (Hitachi S-3400N).

2.6 Enhanced dark field illumination system

Metal nanoparticles were visualized *via* their resonant light scattering using an enhanced dark field (EDF) illumination system (CytoViva, Auburn, AL) attached to a Nikon Optiphot-2 microscope. The system consisted of a CytoViva 150 dark field condenser in place of the microscope's original condenser, attached *via* a fiber optic light guide to a Solarc 24W metal halide light source (Welch Allyn, Skaneateles Falls, NY). In addition, integral to the system was a 100X oil objective with an iris (Olympus UPlanAPO fluorite, N.A. 1.35–0.55). A drop of the NP-reacted cell suspension was added to poly-L-lysine-coated microscope slides (Superfrost Plus, Fisher Scientific, Pittsburgh, PA) and samples were viewed as wet mounts, using Type A (nd >1.515) immersion oil. In some experiments, NP-reacted suspensions of *C. albicans* were also examined using standard light or fluorescence microscopy (Leitz LaborLux S) for comparison with enhanced dark field microscopy (EDFM).

2.7 Digital photography and image processing

Digital images were taken using a consumer-grade digital camera (Canon PowerShot A640) controlled by Axiovision software (v. 4.6, Carl Zeiss Microimaging, Thornwood, NY). In some experiments, we examined the use of a polarizer/analyzer filter set in an effort to minimize image "fuzziness" due to scattered light. Briefly, a polarizer filter was placed at the junction of the light guide and the condenser, and an analyzer (25.4-mm linear glass polarizing filter, Edmund Optics, Barrington, NJ) was placed in front of the camera lens, inside the phototube. Post-capture image processing was also applied to some files. Specifically, we used the "2D Blind Interactive" deconvolution setting of AutoQuant X software (v. 2.0, Media Cybernetics, Bethesda, MD), with 50 iterations.

3 Results and discussion

In the initial phase of this work, we examined a series of 13 commercially available metal NP catalysts, including single-metal and bi- or tri-metallic alloy NP, for their antifungal activities against *C. albicans* using a broth microdilution assay. We found a diverse range in activities for these materials. For single-metal NP, the hierarchy of activity was found to be Co (most effective) > Cu > Ag > Ni > Mn = Pd > Fe (least effective). For alloy NP, it was Co-Ni-Mn (most effective) > Co-Fe > Cu-Ag = Cu-In > Mn-Fe = Ni-Fe (least effective). We had previously determined for silver and other antibacterial NP that physical agitation (shaking) of NP-treated bacterial cultures results in faster kinetics of inactivation than exposure to these NP under static conditions (Weinkauff and Brehm-Stecher, unpublished results). Because only modest agitation resulted in greatly increased kill rates, and because the NP are expected to be too small to cause direct impact damage to cells, these effects were presumed to stem from increased NP-cell interactions brought about by shaking. These results suggest that for any type of NP, direct and sustained physical contact with cell surfaces is probably required for maximal antimicrobial effects. Because the NP in our panel were chemically different from each other (comprised of different elements or elemental mixtures), we expected that they might also have different surface properties, such as the presence or absence of an oxide layer, that might affect their interactions with and binding to *C. albicans* hyphae and cells. We hypothesized that the NP that bound most avidly to *C. albicans* surfaces would also be the most antifungal.

Initially, we sought to demonstrate and characterize NP-*Candida* interactions using SEM, so that we could compare these binding results with our culture-based antifungal data as a test of our hypothesis. Our results for the cobalt NP agreed with our expectations for binding vs. activity relationships – MIC results indicated that these NP were potentially antifungal (MIC of 0.24 ppm) and their interactions with *Candida* surfaces, as determined by SEM, were marked by aggressive coating and encrustation of hyphae and cells (Figs. 1B and D). However, our results for the copper NP were unexpected – although these NP were highly antifungal (MIC of 15.63 ppm), hyphae and cells treated with these NP (Fig. 1C) did not look appreciably different from the no-NP controls (Fig. 1A), as viewed using SEM. Preparation of samples for SEM is a multi-step process involving exposure to multiple chemicals (aldehyde fixatives, osmium tetroxide, ethanol, etc.) and no fewer than seven rinse steps.

We had expected that treatment with cross-linking fixatives such as glutaraldehyde would “cement” bound NP in place and prevent them from sloughing off during sample preparation. Assuming that binding of NP to fungal surfaces is required for activity, our results for copper NPs suggested that fixation with glutaraldehyde was not sufficient to prevent subsequent loss of bound NP from *Candida* surfaces during processing for SEM. In some photos, we saw what appeared to be large flocs of NP close to, but not directly attached to hyphae and cells (data not shown). These observations further suggested that the lack of visible binding we observed for these NP was an artifact originating from loss of binding during sample preparation.

Because our SEM-based approach appeared to be ineffective at detecting some NP-*Candida* interactions, and was time-consuming, we sought to develop an alternative approach for assessing binding of NP to fungal structures. Ideally, such a method would be rapid (*i.e.* faster than the 24-h method used to determine MIC) and would provide direct visual evidence of NP-*Candida* interactions. Other modes of microscopy that have been used previously to study NP-cell interactions include differential interference contrast (DIC) microscopy, and evanescent field-based approaches such as total internal reflection (TIR) or near-field scanning optical microscopy (NSOM) [10, 11]. However, these are high-end analytical approaches, out of reach of most non-specialist labs.

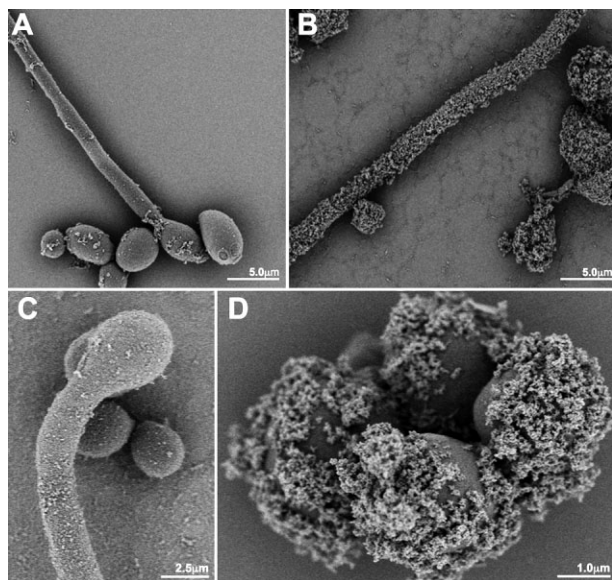


Figure 1. Scanning electron microscopy (SEM) results. Panel A, untreated (control) hyphae of *C. albicans*; Panel B, *C. albicans* hyphae treated with 250 ppm cobalt NP (visible encrustation of NP); Panel C, detail of cobalt-encrusted *C. albicans* cells; Panel D, copper-treated hyphae and cells of *C. albicans* (little or no binding observed *via* SEM).

Our search for an accessible and rapid alternative approach for imaging NP-*Candida* interactions led us to evaluate the CytoViva 150 EDFM system for this purpose. All 13 types of metal NP that we examined yielded bright optical signals when prepared as wet mounts and examined *via* EDFM. For nanometer-scale NP and NP aggregates, we assume that these optical signals arose from surface plasmon-based resonant light scattering effects, a phenomenon that has been well described for silver and gold NP [12, 13]. It is possible, however, that some portion of the signal from larger (*i.e.* micron-range) NP aggregates (iron or copper-indium, for example) may also have resulted from additional light scatter mechanisms governing larger-scale objects. Wet mounts of NP suspensions viewed using EDFM were visually striking, resembling a deep field of stars, with the different intensities and colors of light likely reflecting the sizes of the NP or NP aggregates responsible for each signal (Fig. 2). Our ability to view all types of NP in suspension *via* EDFM suggested that this method would enable us to visualize discrete binding interactions between NP and *Candida* surfaces.

When viewed *via* EDFM, hyphae and cells of *C. albicans* without addition of NP appeared as smooth objects, self-luminous at the edges, with some internal structure visible (septation and microbodies) (Fig. 3). In initial experiments with a small set of metals, we found that an NP level of 250 ppm and a reaction time of 15 min allowed us to visually estimate NP-binding avidity. These conditions were therefore used for evaluation of all NP. For most single-metal NP, the degree of interaction



Figure 2. Wet mount of copper particles viewed *via* enhanced dark field microscopy. This figure highlights the non-quenching resonant light scattering characteristic of the metal NP used in this study. Wet mounts of NP resembled a deep field of stars, with the different intensities and colors of light likely reflecting the sizes of the NP or NP aggregates responsible for each signal.

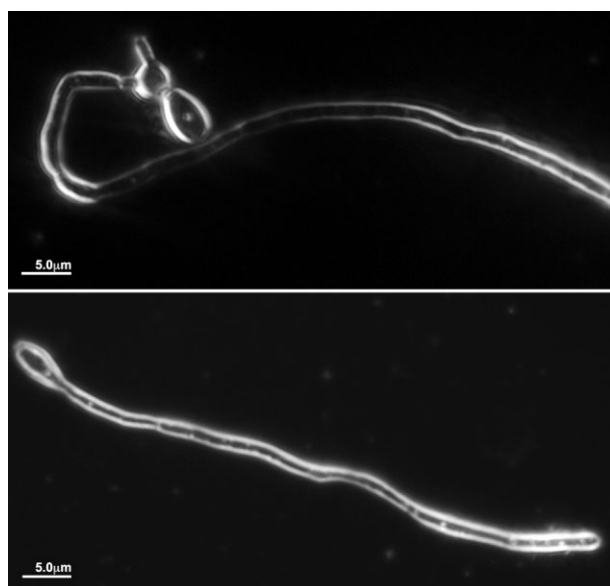


Figure 3. Control hyphae of *C. albicans* (no NP added), viewed *via* enhanced dark field microscopy. When viewed *via* EDPM, hyphae and cells of *C. albicans* without added NP appeared as smooth objects, self-luminous at the edges, with some internal structure visible.

of NP with fungal cells and hyphae occurring within 15 min corresponded well with the antifungal activity determined *via* broth microdilution after 24 h (Table 1). For example, cobalt, copper and silver NP were all found to be highly antifungal *via* broth microdilution and when viewed *via* EDPM, the metals' avidity for hyphal or cellular surfaces was visually clear. Although binding of silver (Fig. 4A) and other NP was not detectable *via* light microscopy (LM), it could be seen clearly using EDPM (Fig. 4C). For cobalt, the most potently antifungal metal, hyphal and cellular surfaces were coated with NP, forming an encrustation that was visible *via* light (Fig. 4B), dark field (Fig. 4D) and scanning electron microscopies (Figs. 1B and D). Occasional light-visible macroscopic aggregates seen for some NP were an

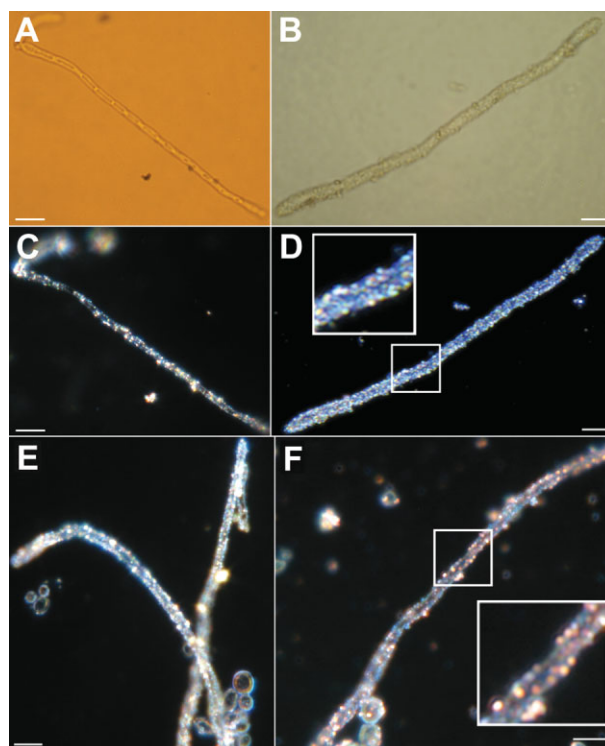


Figure 4. Comparison of NP binding *via* light and enhanced dark field microscopies. Panel A, silver NP (MIC of 31.25 ppm) viewed *via* light microscopy (bound NP not detectable). Panel C, silver NP viewed *via* dark field microscopy (NP easily detected). Panel B, cobalt NPs (MIC of 0.24 ppm) viewed *via* light microscopy (encrustation of cobalt NP visible even *via* light microscopy). Panel D, binding of cobalt NP viewed *via* enhanced dark field microscopy. Inset shows detail of highlighted area, magnified 2.25x. Panel E, copper NP (MIC of 15.63 ppm) demonstrating "bejeweled" appearance. Inset shows detail of highlighted area, magnified 2.5x; Panel F, "bejeweled" appearance of copper-silver alloy NP (MIC of 250 ppm). Scale bars for all panels 5 μ m.

exception to this observation, but even these were not clear *via* LM.

Interestingly, the poorly antimicrobial iron NP or their aggregates emitted an intense, primarily white light, complicating subjective comparisons of binding between this and other NP types (Table 1).

Table 1. Single-metal nanoparticles: binding results at 15 min vs. minimum inhibitory concentration after 24 h

Single-metal NP	Binding result at 15 min <i>via</i> EDPM (relative intensity)	Minimum inhibitory concentration (MIC, ppm)
Cobalt	+++++++	0.24
Copper	++++++	15.63
Silver	+++++	31.25
Nickel	++	250
Manganese	+	1000
Palladium	+++	1000
Iron	++++ ^{a)}	>2000

a) Binding of large, white aggregates.

The relationship between rapid binding and antifungal activity was not as clear for alloy NP, although the intense binding and highly antifungal nature of cobalt dominated in its alloy with the less avidly binding, poorly antifungal metals nickel and manganese (Table 2). Similar effects on binding enhancement may have also been in effect for the manganese-iron and nickel-iron alloys. Individually, all three of these metals had poor activities against *Candida*, but as noted above, iron alone attached well to fungal surfaces, and may have conferred enhanced binding on its manganese or nickel alloys. These results imply a more complex relationship between NP binding and activity than we originally hypothesized, suggesting that NP characteristics not involved in antifungal activity can confer the ability of certain NP to bind to cells. We maintain, however that direct and avid contact of NP with cells is an important factor in mediating antifungal activity, but concede that binding alone may not be sufficient for such activity, as some metals appeared to be intrinsically inactive against this strain of *C. albicans*. For all types of NP, resonant light scattering was not subject to photobleaching and NP were not detectable *via* fluorescence microscopy. Collectively, these data highlight the value of EDFM for visualizing discrete NP-cell interactions that were not visible using either SEM or the other real-time microscopy formats evaluated here.

For the most antimicrobial NP, hyphae and cells took on a dazzlingly bright, “bejeweled” appearance (Figs. 4E and F). Unfortunately, we were unable to capture this effect exactly, as it appeared through the microscope’s oculars. To improve image quality, and reconstruct as closely as possible the images seen through the microscope oculars, we used pre-imaging and post-capture approaches for minimizing haziness and wash, including the use of polarizing filters, post-imaging contrast adjustment and image deconvolution, as described in Section 2.7. While some interference from out of focus light is characteristic of traditional dark field microscopy

[14], the EDFM system used here provides a shallow plane of focus and therefore represents an improvement over traditional dark field approaches, which image an infinite field of depth. Still, our attempts at minimizing the impact of scattered light on image quality were only moderately successful.

While all the NP examined here were visible *via* EDFM, some metals were distinctive, either in coloration or in mode of binding. In addition to the bright, multi-colored encrustations exemplified by cobalt, copper, silver and the copper-silver alloy (Figs. 4C–F), the copper-indium alloy, bound sparsely as large, white globular aggregates (Fig. 5). Although at the macroscale, all NP were indistinguishable from each other as uniform black powders, the different antifungal activities found *via* broth microdilution and binding characteristics seen *via* EDFM highlight their underlying chemical differences, including, potentially, differences in surface chemistries (*i.e.* presence or absence of oxide layers) or electronic properties.

In one experiment, we sought to capture images that could be used to explore the range of colors observed within NP-encrusted or “bejeweled” hyphae (Fig. 6). To do this, we used a combination of pre- and post-processing techniques. Specifically, the image in Fig. 6 was captured using a polarizer/analyzer filter pair (panel A), followed by manual adjustment of contrast in Photoshop CS3 to remove haze (panel B), with a final deconvolution step performed in AutoQuant X v. 2.0 (panel C). The result is a clearer image that displays the range of colors visible on the surfaces of *C. albicans* hyphae reacted with this NP. If larger particles or aggregates yield red-shifted colors [15], then this type of patchwork color pattern might contain information about the localized concentration of NP at the hyphal surface, although the heterogeneity of NP size (~10–100 nm as determined by transmission electron microscopy, TEM) and the depth and availability to incident light of the “crust” may limit such simple analyses. Combination of EDFM with high-end image capture and analysis tools has the po-

Table 2. Metal alloy nanoparticles: binding results at 15 min *vs.* minimum inhibitory concentration after 24 h

Metal alloy NP (1:1:1 or 1:1 ratios)	Binding result at 15 min <i>via</i> EDFM (relative intensity)	Minimum inhibitory concentration (MIC, ppm)
Cobalt/nickel/manganese	+++++	0.49
Cobalt/iron	+++	62.5
Copper/silver	+++++	250
Copper/indium	+++ ^{a)}	250
Manganese/iron	++++	2000
Nickel/iron	+++	2000

a) Sparse binding of large aggregates

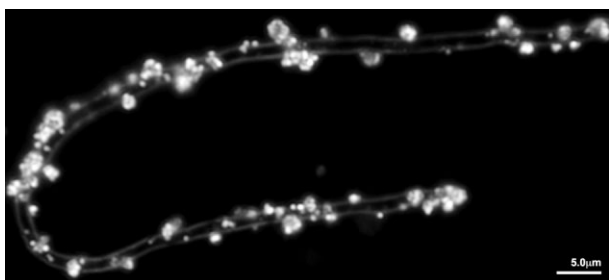


Figure 5. Unique binding profile for copper-indium NP. Sparse binding of large, bright copper-indium NP aggregates.

tential to maximize the value of this approach for monitoring NP-fungal interactions. For example, in the hands of a specialist lab with hyperspectral imaging capabilities and advanced particle recognition software, it may be possible to count particles or estimate their sizes, as well as to conduct time-resolved studies of particle-cell interactions at either brief time scales (*i.e.* initial NP binding dynamics, measured within the first few seconds) or over longer periods (*i.e.* physiological responses of *Candida* to NP exposure over the course of a few hours). Indeed, these types of analyses may already be outside the exclusive realm of specialist imaging labs. The CytoViva® instrument is now available with a hyperspectral imaging spectrophotometer that operates across the visible and near-infrared range (400–1000 nm) and advanced image cytometry software, such as CellProfiler is now available online as open-source freeware (<http://www.cellprofiler.org>). An image cytometry approach has already been used for high content analysis of neuroglioma cells exposed to copper oxide NP [16], but this type of approach might also be used in conjunction with EDFM for direct image cytometry of NP-cell interactions, enabling quantitative analyses of these phenomena.

Typically, plasmon resonance-based imaging of metal NP is carried out using 75–100 W halogen light sources; combined with a 100X 0.9 NA objective, a single non-photobleaching ~80-nm NP illuminated under these conditions can emit $\sim 10^7$ photons/s, the equivalent of ~ 5 million fluorescein molecules [12]. Both the spectra and cross-sectional scattering intensity of these NP change with increasing particle size, providing a means for obtaining NP that emit specific visible colors [13, 15]. These properties make metal NP potentially very valuable as ultra-bright, non-bleaching labels for biological or chemical detection assays, or as we have demonstrated here, as self-reporting labels for NP-cell interactions. The relatively low-power (24 W) EDFM system used here can be operated in

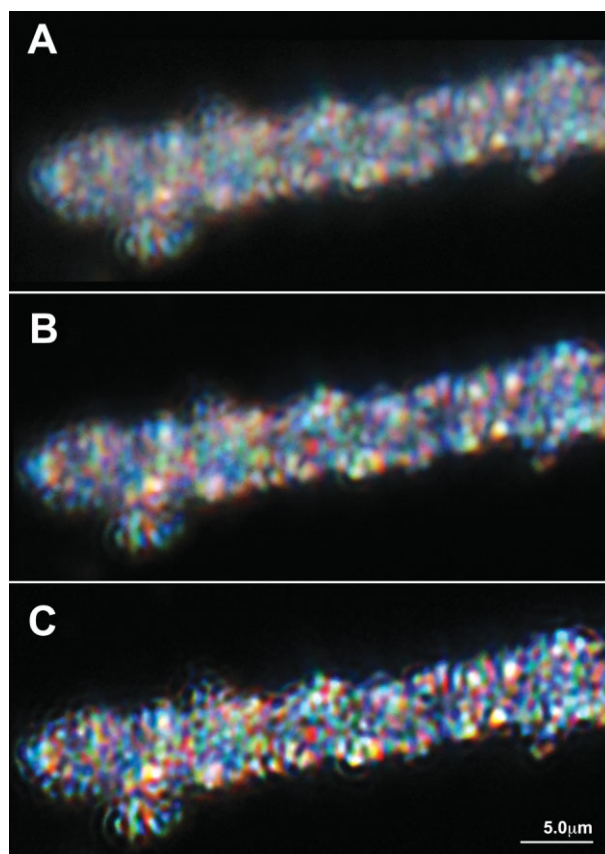


Figure 6. Detail of visible NP colors for cobalt-encrusted hyphum subjected to pre- and post-imaging adjustment and processing. A photo of this cobalt-treated hyphum was captured using a polarizer/analyzer filter set (panel A). The image was contrast-adjusted in Adobe Photoshop CS3 to remove visible haze (panel B). Image deconvolution (AutoQuant X v. 2.0) was then used to further sharpen features, as described in the text (panel C). The result is a clearer image highlighting the range of colors comprising the “bejeweled” phenotype of binding seen for cobalt NP.

two basic modes - a detection mode, where objects as small as 20 nm can be seen and information on their movement, interaction or aggregation can be collected, and an imaging mode, where structures as small as 90–100 nm can be optically resolved [17, 18]. Beyond facilitating resolution of very small features using a standard research-grade light microscope, the EDFM instrument we used can also elicit and detect fluorescence [19]. While we did not utilize the instrument’s fluorescence capabilities in this work, the capacity for simultaneous resonant light scattering/fluorescence imaging opens up potentially useful future possibilities for imaging NP-cell interactions (see “Concluding remarks”, below).

Although we typically consider nanotechnology to be a new (and still emerging) field, studies on nano-optical phenomena were already being car-

ried out at the turn of the 20th century. Heinrich Siedentopf and Richard Zsigmondy developed the dark field “ultramicroscope” for optical detection and characterization of colloidal metals (metal NP), and Zsigmondy won the 1925 Nobel Prize in Chemistry for his work on colloids [20, 21]. Unfortunately, interest in use of the ultramicroscope waned with the invention of the electron microscope in the early 1930’s [20]. However, today’s “nanotech revolution” has fueled renewed interest in dark field microscopy, due to its usefulness in investigating the optical properties of nanomaterials [12, 13, 20]. Our use of the ultramicroscopy-like detection mode EDFM echoes the pioneering work of Zsigmondy, who observed that “...isolated particles, whose diameter is a fraction of a wave-length of light, can still be seen...” using this technique [21]. Other microscopic approaches that may also be of value for examining NP-cell interactions include the DIC, TIR and NSOM methods mentioned above as well as the recently described single-plane or selective-plane imaging microscopy (SPIM), also known as “light sheet” microscopy [22, 23]. SPIM, which has its origins in Siedentopf’s and Zsigmondy’s ultramicroscope, is essentially a method for optical tomography, whereby discrete planar “slices” of the sample can be selectively imaged, reducing the background signal from objects outside of the focal plane and causing fewer problems with photobleaching or photodamage [23]. In SPIM, light from a laser source is optically focused into a thin “sheet” of light that overlaps with the focal plane in the sample, which is immersed in liquid or embedded in a transparent hydrogel having the same refractive index as water [22, 23]. Instead of moving the light sheet, the sample itself is translated or rotated to provide the desired sectioning of the sample [23]. Variant approaches of the same basic technology exist, with the chief differences being horizontal vs. vertical sectioning, sample embedding vs. liquid immersion and single-sided vs. dual-sided excitation [22, 23]. Because it is a form of optical tomography, multiple SPIM images can be stacked to provide a reconstruction of the original sample [22, 23]. Although it has been described primarily for optical sectioning of larger cells or embryos, SPIM has also been described for yeast [23] and a very similar approach has been taken for the study of naturally occurring aquatic microbes [24].

With their abilities to perform optical sectioning of the sample, SPIM-based approaches may be useful for investigating NP-*Candida* interactions. Using the EDFM method described here, we were only able to get a “top-down” view of NP-coated cells and hyphae, and information on NP distribu-

tion over the entire curved surfaces of *Candida* structures was not available. Using an SPIM approach, NP-*Candida* complexes could potentially be sectioned, with a 1.5- μm light sheet yielding ~six sections per sample [23]. This multiplanar view could provide information on surface-bound (or internalized) NP throughout the volume of the cell or hyphum. Although a commercial SPIM instrument is in development, the availability of this technology is limited, as the only instruments now in existence are those custom-built by specialist labs. Additionally, unlike EDFM, we do not know the extent that the SPIM architecture would support generation of dynamic light scattering from metal NP. Therefore, although the EDFM approach may not be the only solution to investigating NP-*Candida* interactions, it does have the added benefits of being accessible and easy to use and is available as a modular upgrade to most existing light microscopes, taking the place of the microscope’s original condenser.

4 Concluding remarks

We have described a rapid, microscopic method for visualizing interactions between metal NP and fungal hyphae based on resonant light scattering of these particles when viewed using EDFM. This approach grew out of a need for rapid and direct visualization of NP-fungal interactions, without the extensive preparative steps used in SEM that could lead to artifacts, such as sloughing of bound NP during sample preparation. Although we ultimately found that the relationship between NP-binding and antifungal activity was not as direct as we had originally hypothesized, our work demonstrates the use of EDFM for detecting and characterizing binding interactions between metal NP and fungal hyphae or cells, a result that could be useful in further characterization of these NP as antimicrobials or in future applications of similar NP as non-chemical, non-quenching labels for microbial diagnostics. Although binding alone was not a sufficient metric for assessing the antimicrobial capacity of the NP examined here, the EDFM approach used here could be expanded for more detailed studies of NP activity at fungal surfaces. In addition to surface plasmon effects, the CytoViva[®] instrument used here is also able to elicit fluorescence, opening the possibility for combination of these modalities for correlative studies on binding of NP to cells and their subsequent physiological effects. For example, in future studies, it may be possible to combine EDFM with appropriate fluorescent probes in order to examine the physiological pathways

through which antifungally active NP exert their effects. Example probes might include fluorescent respiratory substrates or free radical indicators [4, 25]. More detailed insights might also be possible using engineered microbial strains capable of fluorescently reporting perturbations of major cellular biosynthetic pathways, including synthesis of DNA, RNA, proteins, fatty acids and the cell wall [26].

We thank QuantumSphere, Inc. (Santa Ana, CA) for supplying the nanoparticles used in this study, CytoViva® Inc. (Auburn, AL), for use of a CytoViva® high-resolution dark field condenser and Jean Ross at the University of Iowa's Central Microscopy Research Facility (CMRF, Iowa City, IA) for her expert electron microscopy work. Funding for this work was provided by QuantumSphere, Inc., by an award to BFBS from Iowa State University's Office of Biotechnology and by USDA National Needs Fellowship Grant No. 2005-02324.

The authors have declared no conflict of interest.

5 References

- [1] Borkow, G., Gabbay, J., Copper as a biocidal tool. *Curr. Med. Chem.*, 2005, 12, 2163–2175.
- [2] Noyce, J. O., Michels, H., Keevil, C. W., Use of copper cast alloys to control *Escherichia coli* O157 cross-contamination during food processing. *Appl. Environ. Microbiol.* 2006, 72, 4239–4244.
- [3] Santo, C. E., Taudte, N., Nies, D. H., Grass, G., Contribution of copper ion resistance to survival of *Escherichia coli* on metallic copper surfaces. *Appl. Environ. Microbiol.* 2008, 74, 977–986.
- [4] Kim, J. S., Kuk, E., Yu, K. N., Kim, J.-H. *et al.*, Antimicrobial effects of silver nanoparticles. *Nanomedicine* 2007, 3, 95–101.
- [5] Skebo, J. E., Grabinski, C. M., Schrand, A. M., Schlager, J. J. *et al.*, Assessment of metal nanoparticle agglomeration, uptake, and interaction using high-illuminating system. *Int. J. Toxicol.* 2007, 26, 135–141.
- [6] Lok, C.-N., Ho, C.-M., Chen, R., He, Q.-Y. *et al.*, Proteomic analysis of the mode of antibacterial action of silver nanoparticles. *J. Proteome Res.* 2006, 5, 916–924.
- [7] Kim, K.-J., Sung, W. S., Suh, B. K., Moon, S.-K. *et al.*, Antifungal activity and mode of action of silver nano-particles on *Candida albicans*. *Biometals* 2008, DOI 10.1007/s10534-008-9159-2.
- [8] Lambert, R. J., Johnston, M. D., Simons, E.-A., Disinfectant testing: use of the bioscreen Microbiological Growth Analyzer for laboratory biocide screening. *Lett. Appl. Microbiol.* 1998, 26, 288–292.
- [9] National Committee for Clinical Laboratory Standards. 2002. Reference method for broth dilution antifungal susceptibility testing of yeasts. Approved standard M27-A2. National Committee for Clinical Laboratory Standards, Wayne, Pa.
- [10] Pelton, M., Aizpurua, J., Bryant, G., Metal-nanoparticle plasmonics. *Laser & Photon. Rev.* 2008, 2, 136–159.
- [11] Sun, W., Fang, N., Trewyn, B. G., Tsunoda, M. *et al.*, Endocytosis of a single mesoporous silica nanoparticle into a human lung cancer cell observed by differential interference contrast microscopy. *Anal. Bioanal. Chem.* 2008, 391, 2119–2125.
- [12] Schultz, S., Smith, D. R., Mock, J. J., Schultz, D. A., Single-target molecule detection with nonbleaching multicolor optical immunolabels. *Proc. Natl. Acad. Sci. USA* 2000, 97, 996–1001.
- [13] Schultz, D. A., Plasmon resonant particles for biological detection. *Curr. Opin. Biotechnol.* 2003, 14, 13–22.
- [14] Hazelwood, K. L., Olenych, S. G., Griffin, J. D., Cathcart, J. A. *et al.*, Entering the portal: understanding the digital image recorded through a microscope. In: Frischknecht, F., Shorte, S. L. (Eds.), *Imaging Cellular & Molecular Biological Function*, Springer-Verlag, Berlin 2007, pp. 33–34.
- [15] Kyriacou, S. V., Brownlow, W. J., Xu, X.-H. N., Using nanoparticle optics assay for direct observation of the function of antimicrobial agents in single live bacterial cells. *Biochemistry* 2004, 43, 140–147.
- [16] Li, F., Zhou, X., Zhu, J. Ma, J. *et al.*, High content image analysis for H4 human neuroglioma cells exposed to CuO nanoparticles. *BMC Biotechnol.* 2007, 7, 66 doi:10.1186/1476-6750-7-66.
- [17] Vainrub, A., Pustovyy, O., Vodyanoy, V., Resolution of 90 nm ($\lambda/5$) in an optical transmission microscope with an annular condenser. *Opt. Lett.* 2006, 31, 2855–2857.
- [18] Guntupalli, R., Sorokulova, I., Krumnow, A., Pustovyy, O. *et al.*, Real-time optical detection of methicillin-resistant *Staphylococcus aureus* using lytic phage probes. *Biosens. Bioelectron.* 2008, 24, 151–154.
- [19] Brehm-Stecher, B. F., New technologies for imaging individual microbial cells. In: Frischknecht, F., Shorte, S. L. (Eds.), *Imaging Cellular & Molecular Biological Function*, Springer-Verlag, Berlin 2007, pp. 313–343.
- [20] Kreibitz, U., Gartz, M., Hildger, A., Hövel, H. *et al.*, A short survey of optical properties of metal nanostructures. In: Kassing, R., Petkov, P., Kulisch, W., Popov, C. (Eds.), *Functional Properties of Nanostructured Materials*, Springer-Verlag, Berlin 2006, pp. 75–110.
- [21] Zsigmondy, R., Facts pointing to the homogeneity of gold hydrosols. Development of ultramicroscopy. In: Alexander, J. (Transl.), *Colloids and the Ultramicroscope: a Manual of Colloid Chemistry and Ultramicroscopy*, John Wiley & Sons, New York 1909, p. 101.
- [22] Dodt, H.-U., Leischner, U., Schierloh, A., Jährling, N. *et al.*, Ultramicroscopy: three-dimensional visualization of neuronal networks in the whole mouse brain. *Nat. Methods* 2007, 4, 331–336.
- [23] Reynaud, E. G., Krzic, U., Greger, K., Stelzer, E. H. K., Light sheet-based fluorescence microscopy: more dimensions, more photons, and less photodamage. *HFSP J.* 2008, 2, 266–275.
- [24] Fuchs, E., Jaffe, J. S., Long, R. A., Azam, F., Thin laser light sheet microscope for microbial oceanography. *Opt. Express* 2002, 10, 145–154.
- [25] Kohanski, M. A., Dwyer, D. J., Hayete, B., Lawrence, C. A. *et al.*, A common mechanism of cellular death induced by bactericidal antibiotics. *Cell* 2007, 130, 797–810.
- [26] Urban, A., Eckermann, S., Fast, B., Metzger, S. *et al.*, Novel whole-cell antibiotic biosensors for compound discovery. *Appl. Environ. Microbiol.* 2007, 73, 6436–6443.